Progress in Additive Manufacturing
https://doi.org/10.1007/s40964-024-00691-0

FULL RESEARCH ARTICLE

Energy absorption characteristics and deformation mechanism of TPMS and plate-lattice-filled thin aluminum tubes

Ali N. Alagha[1,2] · Jamal Y. Sheikh-Ahmad[1,2,3] · Firas Jarrar[1,2,4] · Fahad Almaskari[1,2] · Rashid K. Abu Al-Rub[1,2]

Received: 9 October 2023 / Accepted: 2 June 2024

Abstract

In recent years, thin-walled structures filled with various materials and structures have been of interest due to their high energy absorption efficiency and lightweight. The current developments in additive manufacturing technologies provide a useful tool to produce low-density core materials to improve the energy absorption performance of thin-walled structures. For that purpose, lattice filled thin-walled structures with two types of periodic shellular materials (i.e., diamond TPMS and SC-FCC-BCC plate-lattice) were proposed, and the effect of various design parameters, including tube thickness and height, on the energy absorption characteristics was tested under quasi-static loading and validated using finite element analysis (FEA) and homogenization techniques. Diamond cylindrical core lattices developed diagonal shear bands at the early loading stages, while the constituting plates of SC-FCC-BCC lattice tended to bend toward the loading direction. As a result of their lower degree of buckling, short hybrid samples showed a higher ability to absorb energy as compared to long samples because of the larger induced interaction effect between the considered cores and tubes. These effects were due the variations in the deformation mechanism, which subsequently led to an increase in the energy absorption of the structures. From an energy absorption perspective, the optimal hybrid structure design with maximum specific energy absorption was found to be at 1 mm short hybrid tube samples for both SC-FCC-BCC plate-lattice (22.7 J/g) and diamond TPMS (18.6 J/g). This study demonstrates the potential of employing these structures in sectors where high energy absorption is necessary, including automotive, aerospace, and protective structures and are, thus, recommended as promising candidates for crashworthiness applications.

Keywords Triply periodic minimal surface (TPMS) · Plate-lattices · Additive manufacturing · Metamaterials · Homogenized core · Lattices

1 Introduction

For the case of impact loading protection, thin-walled structures come as the most prominent choice due to their combined properties of high energy absorption, low cost, lightweight and ease of manufacturing [1–3]. These structures are recognized for their exceptional energy absorption to mass ratio, enhancing reliability in sectors where structural mass is critical [4]. Thin-walled structures are increasingly recognized for their potential across multiple industries due to their unique combination of properties [1, 5–8]. In the automotive sector, they improve vehicle safety and fuel efficiency by enhancing crashworthiness while maintaining lightweight [9, 10]. In aerospace industry, they contribute to the enhancement of lightweight design in aircraft components [11]. Civil engineering also benefits from their use in impact-resistant barriers and protective building panels,

✉ Rashid K. Abu Al-Rub
rashid.abualrub@ku.ac.ae; rashedkamel@yahoo.com

1 Advanced Digital & Additive Manufacturing Center, Khalifa University of Science and Technology, Abu Dhabi, United Arab Emirates

2 Department of Mechanical Engineering, Khalifa University of Science and Technology, P.O. Box 127788, Abu Dhabi, United Arab Emirates

3 Department of Mechanical Engineering, Western New England University, P.O. Box 01119-2684, Springfield, USA

4 Mechanical Engineering Department, AlHussein Technical University, Amman, Jordan

Published online: 12 June 2024

offering both strength and durability under dynamic loading conditions [12]. Additionally, in the biomedical field, the high surface area and tailored mechanical properties of thin-walled lattice structures are advantageous in designing implants that mimic the mechanical properties of bones, promoting better integration and longevity of the implants [13, 14].

Although thin-walled structures show immense potential in terms of energy absorption, their impact loading stress–strain curves display a high peak followed by a sharp drop, indicating an undesirable reduction in the structure's strength. To avoid such behavior, the development of thin-walled structures with unique designs has been of interest to many researchers. For that purpose, various cross-sectional shapes (e.g., circular, rectangular, triangular), materials (e.g., corks, composites, steel), and geometric patterns (e.g., functionally graded, windowed) were proposed [15–20].

Attempts to improve the crashworthiness of the thin-walled tubes were carried out by filling the tubes with different types of low-density porous materials, such as foams and lattice structures [21, 22]. Several studies revealed that the foam-filled tubes improve the crushing performance as compared to empty tubes [23–25]. These improvements were related to the advantageous modifications in the buckling modes of the structure, reducing its buckling length by inner foam interactions with the thin-walled structure. The interaction effects between the filler foams/lattices and the supporting structures result in desirable characteristics in terms of energy absorption and mass specific properties. While aluminum foams have drawn growing attention due to their lightweight properties and stable deformation [22], a limitation of such foams is their low crushing strength which results in a limited energy absorption capacity per unit volume [16, 24]. Some alternative cores that can be utilized are lattice structures that provide a high capability to absorb mechanical loading combined with lightweight and stiffness, making them desirable for energy absorption devices [26–31]. As a result of the structural complexity and fabrication difficulties, lattice structures as inserts were not widely utilized in engineering applications. With the rapid development of additive manufacturing (AM), fabrication and testing of such lattices became effortlessly possible [32]. As such, works related to additively manufactured lattice-filled tubes were recently explored in the literature. The most widely studied lattices as thin-walled structures cores are honeycombs and trusses. Each of these structures has its own unique behavior and advantages. Since 2D cellular structures suffer from unstable deformation and premature failure, honeycombs are commonly combined with thin-walled components as hybrid structures. In this regard, Liu et al. [33] investigated the influence of combining carbon fiber reinforced polymer (CFRP)-based square tubes with aluminum-based honeycomb structures under axial loading. The authors noted a slight increase of about 2% in specific energy absorption (SEA) as compared to the empty tubes, with high dependence on the cell width of the inner lattice. Combining different materials might result in distinct properties. For instance, low-carbon steel square tubes and Vero Gray Full Cure 850 honeycomb cores resulted in 28% increase in SEA [34], while 23% increase was reported for aluminum honeycomb and square tubes [35]. The wide variations were attributable to the differences in the interactions between the inner lattice structure and the tube, based on the material considered. A disadvantage of honeycombs however, is their high anisotropy [36], which is considered as a huge limitation when used for energy absorption. Truss lattices, on the other hand, outperform honeycombs in terms of specific strength and stiffness [37]. These structures were often combined with thin-walled structures as energy absorption devices. In their most recent works, Cetin et al. [38–40] investigated the mechanical behavior of aluminum-based body-centered cubic (BCC) and body-centered cubic with vertical struts (BCC-Z) as fillers in squared AlSi10Mg tubes under axial impact loading. It was noted that the tube and the inner lattice highly contribute to the buckling behavior of each other, having energy absorption improved with the optimization of the tube thickness and the inner core design. Additionally, Liu et al. [41] analyzed the behavior of aluminum-based BCC lattices as core structure of single, double, and multi-cell tubes with different aspect ratios. They noted a higher energy absorption efficiency as either strut size increased or aspect ratio reduced, which was a result of the low levels of buckling associated with both cases.

From an energy absorption efficiency perspective, the abovementioned structures do not possess the utmost energy absorption capabilities as compared to the newly developed triply periodic minimal surfaces (TPMS) [42, 43] and plate-lattices [44]. TPMS structures are well known for their superior mechanical properties as compared to strut-based lattices. Furthermore, the plate-lattices were also characterized with outstanding stiffness and mechanical energy absorption performance, and can be quite comparable with TPMS when hybridized [28]. Indeed, among different plate-lattices, the most promising are the combined unit cells, owing to their high stiffness and energy absorption performance [44]. For that, these lattices can be excellent candidates for lattice-filled thin-walled structures. The utilization of these two lattice types as core material for energy absorption devices is new and not widely explored in literature. Few works have investigated the advantages of adding TPMS as cores to thin-walled structures, while plate-lattices were not considered previously. For the case of TPMS, Novak et al. [45, 46] and Yin et al. [47] experimentally tested the mechanical behavior, under quasi-static and bending loading, of

aluminum-based squared tubes filled with TPMS lattices. A drastic increase in energy absorption was reported, up to 46%, as compared to the sum of empty tube and reference core. Among different TPMS structures, diamond is the most promising in terms of energy absorption [48, 49].

From the abovementioned studies on thin-walled hybrid structures, it can be emphasized that there is a need to further explore the mechanical performance of different combinations of materials, inner lattice designs, and tube cross sections and thicknesses. Due to the importance of energy absorption components, it is a critical challenge to explore the potential advantages of utilizing TPMS lattices and plate-lattices. In this study, diamond TPMS and SC-FCC-BCC plate-lattice-filled tubes were proposed, and their quasi-static mechanical behavior, in terms of deformation mechanism and energy absorption was analyzed for different tube designs. The experimental data were then utilized to validate the developed computational model.

The manuscript is organized as follows: Sect. 2 provides a summary of the materials and methods used to design and characterize the hybrid structure samples, based on factorial design. Section 3 is dedicated to provision of effects of the distinctive design parameters on the deformation mechanism and mechanical behavior of the hybrid structures. Finally, the conclusions, limitations, and outlook of the present work are summarized in Sect. 4.

2 Materials and methods

2.1 Design and fabrication of the samples

The TPMS are surfaces that are defined by zero mean curvature at every domain's point in three dimensions. Plate-lattices are formed by placing plates along planes of a crystal structure. The two studied structures are diamond TPMS and SC-FCC-BCC plate-lattice with a fixed value of relative density and unit cell length. The CAD files of the SC-FCC-BCC plate-lattice were created by combining three types of plate-lattices (i.e., FCC, BCC, and SC) using SOLIDWORKS software. The sheet-based diamond TPMS lattice was generated using MSLattice software, developed by Al-Ketan and Abu Al-Rub [50], using the level-set approximation:

$$\cos x \cos y \cos z - \sin x \sin y \sin z = c, \tag{1}$$

where x, y, z are Cartesian coordinates, and c is a parameter representing the level-set iso-value, which controls the relative density.

The chosen relative densities and unit cell length are $\rho_R = 40\%$ and $L_u = 18$ mm for diamond and $\rho_R = 50\%$ and $L_u = 22$ mm for the plate-lattice, respectively. These values are based on the optimized design for structural specific energy absorption in [51]. The designed cylindrical lattices are shown in Fig. 1.

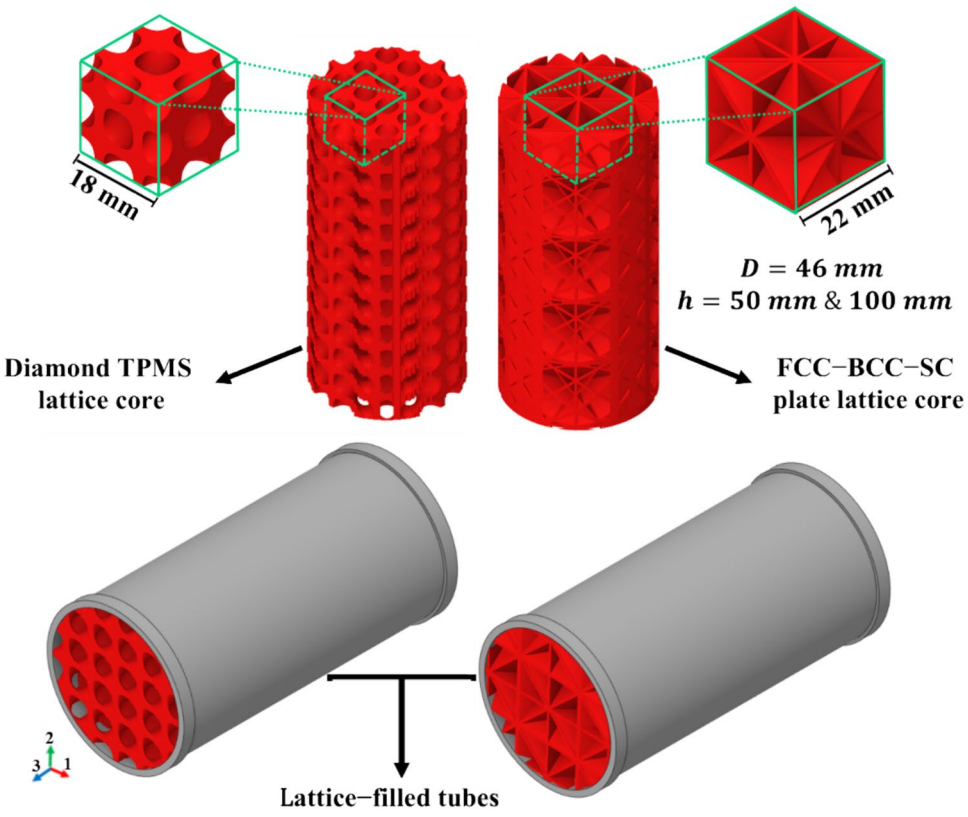

Fig. 1 CAD design of the cylindrical lattices considered ($\rho_R = 40\%$ for diamond and $\rho_R = 50\%$ for the SC-FCC-BCC plate-lattice) and a schematic representation of the designed lattice-filled tubes

Table 1 Properties of 3D printing ABS

Property	Triton™ ABS
Density	1.05 g/cm^3
Tensile strength	30 MPa
Filament diameter	1.75 mm
Glass transition temperature	105 °C

Table 2 Factorial design of experiments

Parameter	Value
Tube thickness [t_T] (mm)	0.50, 0.75, 1.00
Tube height [h_T] (mm)	50, 100
Core structure	Diamond TPMS, SC-FCC-BCC plate-lattice

Different combinations of the presented values were considered for the samples

Three design variables were considered in this work, namely tube height (h_T), tube thickness (t_T), and tube core lattice structure. To fabricate the core structures, fused deposition modeling (FDM) 3D printing technique was employed, comprising of Triton™ Acrylonitrile butadiene styrene (ABS) thermoplastic polymer, via Creatbot F430 3D printer, equipped with 300 × 300 mm build plate. ABS was chosen as the material for the experiments due to its favorable mechanical properties, which makes it suitable for evaluating the mechanical behavior of polymeric 3D-printed cellular materials. The chosen printing parameters were based on an optimization process, utilized following [52]. The extruder temperature was set to 230 °C, while the build plate was heated to 100 °C, the layer thickness and printing speed were set at 0.2 mm and 50 mm/s, respectively. To ensure a high-quality print, the printer capabilities were respected. In particular, a nozzle diameter of 0.4 mm was used, based on the minimum wall thickness of the designed structures (1.2 mm), utilizing a diameter that is at least half of the minimum feature size. The infill parameter was set to 100%, to assure fabricating fully dense sheets or plates in the lattices. The filament material properties are summarized in Table 1.

The extruded tubes were made of Aluminum (Al) 6063-T6. The original thickness of the tube was 2 mm. The tubes were machined to reduce the thickness based on the factorial design of Table 2. Extra thickness at the two ends of the tubes was kept at 2 mm to avoid stress concentration points (Fig. 1), the tubes were then polished to avoid stress concentration. To obtain the material's mechanical properties used in finite element analysis (FEA), a plate of the same material (Al) was purchased and machined into dog bone samples, while ABS tensile samples where additively manufactured with similar process parameters as the lattice core structures. Based on the factorial design, lattice samples with h_T= 50 mm and 100 mm heights were fabricated and inserted into the tubes with different tube thicknesses. The mass of each sample was measured with a 0.001 g accuracy scale to evaluate the mass relative density and specific energy absorption (SEA).

2.2 Experimental testing

Upon fabrication, uniaxial compression was employed to evaluate the effect of distinctive design parameters on the mechanical response of the hybrid cylindrical structures using Instron 5969 universal testing machine. The displacement was reported by measuring the movement of the crosshead and compressive load was measured using a 100 kN load cell. The samples were tested until densification or when a load limit of 95 kN was reached, with a strain rate of 4 mm/min. To ensure repeatability, three replicas of each sample were fabricated and tested. Energy absorption was calculated until the displacement representing the onset of densification, which was accurately evaluated using the efficiency curve criteria [53]. The crushing behavior of all samples was recorded using a high-definition camera to investigate the effect of each parameter considered.

2.3 Finite element analysis (FEA)

FEA and a numerical homogenization technique were utilized to validate the obtained experimental results. Initially, the mechanical properties of aluminum and ABS were obtained by testing dog bone specimens under tension, based on ASTM E8 and ASTM D638 standards, respectively. For the core material, the effective mechanical properties of the two structures were extracted. Following the procedure described by Lee et al. [54], numerical homogenization was firstly carried out using the unit cell method, which takes advantage of the periodicity of the structures to obtain the effective behavior from a single representative cell subjected to periodic boundary conditions. The obtained effective mechanical properties were then utilized to simulate the hybrid structures with a homogenized core, as illustrated in Fig. 2.

For that purpose, the CAD files were exported to Abaqus FEA software. An isotropic, finite strain, elasto-plastic, and rate-independent constitutive material model for both tube and inner core was used. Damage and fracture modeling were ignored in the current study for simplicity, since most of the observed deformation mechanisms are driven by plastic collapse and deformation. A summary of the mechanical properties of Al and effective properties for both diamond and plate-lattice structures cores is provided in Table 3. From this point onwards, the SC-FCC-BCC plate-lattice

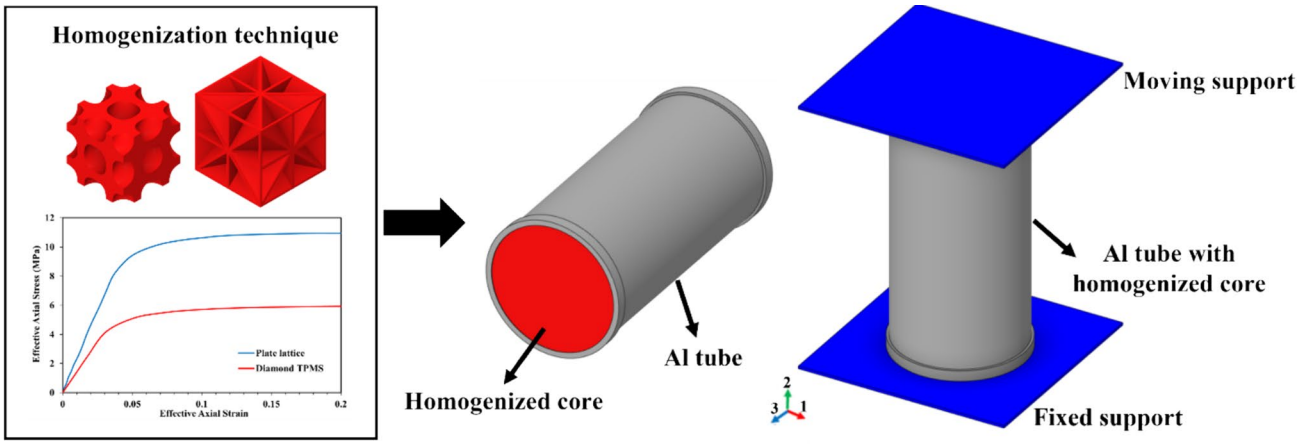

Fig. 2 Schematic representation of the applied boundary conditions for FEA. Homogenization technique was used to obtain the effective properties for the lattice core structure

Table 3 Experimentally obtained mechanical properties utilized in FEA material model

Property	Tubes (Aluminum)	Homogenized diamond (ABS)	Homogenized plate-lattice (ABS)
Young's modulus (GPa)	66.7	–	–
Effective Young's modulus (MPa)	–	2.2	2.4
Yield stress (MPa)	202	–	–
Effective yield stress (MPa)	–	4.4	9.9
Poisson's ratio	0.33	0.35	0.35
Mass density (g/cm^3)	2.7	1.05	1.05

Effective properties were obtained using FEA unit cell method and homogenization technique

and diamond TPMS might be referred to as "PL" and "D," respectively.

A surface contact with friction was defined between the tube and the supports, and a general contact with friction was defined for the tube and core structure. The friction coefficients at the supports and the hybrid structure were set to 0.2 and 0.4, respectively. A quadratic tetrahedral element (C3D10 per Abaqus notion) was utilized for the mesh for both cores and tubes. Mesh sensitivity analysis was conducted until minimal difference in the results was observed.

3 Results and discussion

The mechanical behavior of the lattice-filled tubes was investigated under quasi-static axial loading experimentally and using FEA. The quasi-static loading was first carried out and the force–displacement curves and deformation mechanism of each sample was analyzed for core lattice, empty tubes, and lattice-filled tubes with different thicknesses and heights. The results were then validated using FEA and numerical homogenization. The obtained samples were weighted upon fabrication and the actual mass relative density was evaluated and compared to the CAD models' relative density, as shown in Table 4.

It can be noted from Table 4 that there was a slight deviation in the values of actual mass ρ_R as compared to designed ρ_R, with higher differences for the plate-lattice than diamond structures. These variations were attributed to the discrepancies of walls thickness and other printing defects associated with the process of extrusion-based additive manufacturing. The presence of such defects significantly contributes to the accuracy of fabricated parts, leading to variations in the total volume occupied by the fabricated sample and thus, relative density of the structure. The samples were divided into two groups, long ($h_T = 100$ mm) and short ($h_T = 50mm$) samples. The additively manufactured cylindrical cores and hybrid structures are illustrated in Fig. 3.

Table 4 Measured mass ρ_R of the additively manufactured lattice core structures and the deviation from the originally designed CAD models for the different structures and heights

Sample	L_U(mm)	Designed ρ_R (%)	L_T(mm)	Sample mass (g)	Mass ρ_R (%)	Deviation (%)
Diamond TPMS	18	40	50	35.89 ± 0.08	39.18 ± 0.21	− 2.0
			100	70.04 ± 0.61	39.41 ± 0.86	− 1.5
SC-FCC-BCC plate-lattice	22	50	50	98.06 ± 0.90	51.49 ± 0.92	+ 3.0
			100	49.63 ± 0.40	52.12 ± 0.80	+ 4.2

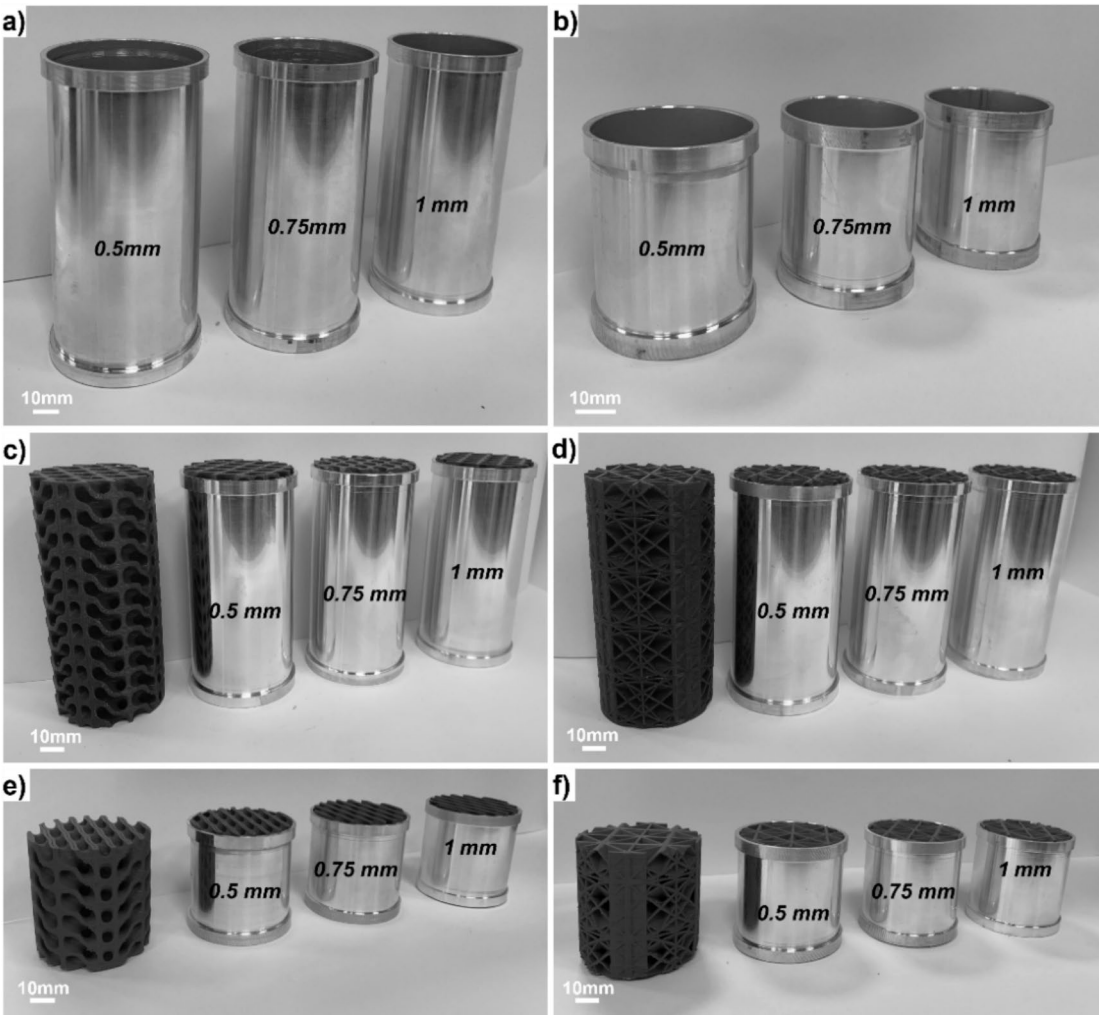

Fig. 3 Tested samples; empty **a** long and **b** short Al tubes; **c** Diamond lattice-filled long Al tubes; **d** SC-FCC-BCC plate-lattice-filled long Al tubes; **e** Diamond-filled short Al tubes; **f** SC-FCC-BCC plate-lattice-filled short Al tubes

3.1 Quasi-static axial loading

3.1.1 Empty tubes mechanical behavior

Reference tubes with different thicknesses and heights were tested to identify the collapse mode based on the design parameters. The inner diameter of all tubes was fixed at 46 mm, while t_T (0.5, 0.75 and 1 mm) and h_T (50 and 100 mm) varied. Two important ratios that predict the deformation mechanism can be calculated for each sample, namely h_T/D and t_T/D, where D represents the inner diameter of the tube (i.e., 46 mm). Based on these ratios, the collapse modes of different structures were examined and plotted by Andrews et al. [55], noting that specific combinations of these ratios trigger certain types of collapse modes. The deformation mechanism based on design parameters follows the same behavior predicted. The obtained deformation mechanism from experiments and FEA at 30% strain level (30 mm

displacement for long tubes and 15 mm for short tubes), in addition to the force–displacement curves of the long and short empty tubes are provided in Fig. 4.

The deformation mechanism is well captured by the computational model (Fig. 4a). For the short samples, tube thickness highly affects the crushing behavior. At $t_T = 0.5$ mm the tubes tend to undergo a mixed mode of deformation, which was indicated by the formation of an axisymmetric ring followed by sequential folding, resulting due to the change of the cross-sectional area of the tube (diamond collapse). As tube thickness increased ($t_T = 0.75$ and 1 mm), the formation of an axisymmetric ring, starting from one end of the tube was obtained. Maximum energy absorption can be achieved by the formation of the so-called concertina rings [20, 31, 55]. The formation of these rings can be confirmed by the development of two consecutive waves with comparable amplitude in the force–displacement curve. For instance, the two consecutive peaks at ~ 11 and 25 mm displacement for the 1 mm tube of Fig. 4b represent the formation of the axisymmetric ring. The long tubes, on the other hand, were characterized by mixed collapse modes at all considered tube thicknesses. Those were represented by a combined formation of axisymmetric rings and diamond folds, which are indicated in the force–displacement curves of Fig. 4c as random peaks and fluctuations. It is worth noting that mixed collapse mode, in general, negatively affects the overall performance of the hybrid structures [31].

3.1.2 Effect of hybrid structure design on the mechanical behavior

In this sub-section, the effects of the parameters studied (i.e., tube thickness, height, and core lattice type) on the mechanical performance of the hybrid structures are presented. The force–displacement curves and crushing behavior are first discussed, and the mechanical properties extracted from the curves are subsequently illustrated.

3.1.2.1 Force–displacement curves and deformation mechanism Experimental and computational mechanical responses, indicated by force–displacement curves for long and short samples with the three considered thicknesses are provided in Figs. 5 and 6, respectively. Simulation curves produced using the homogenization technique follow a

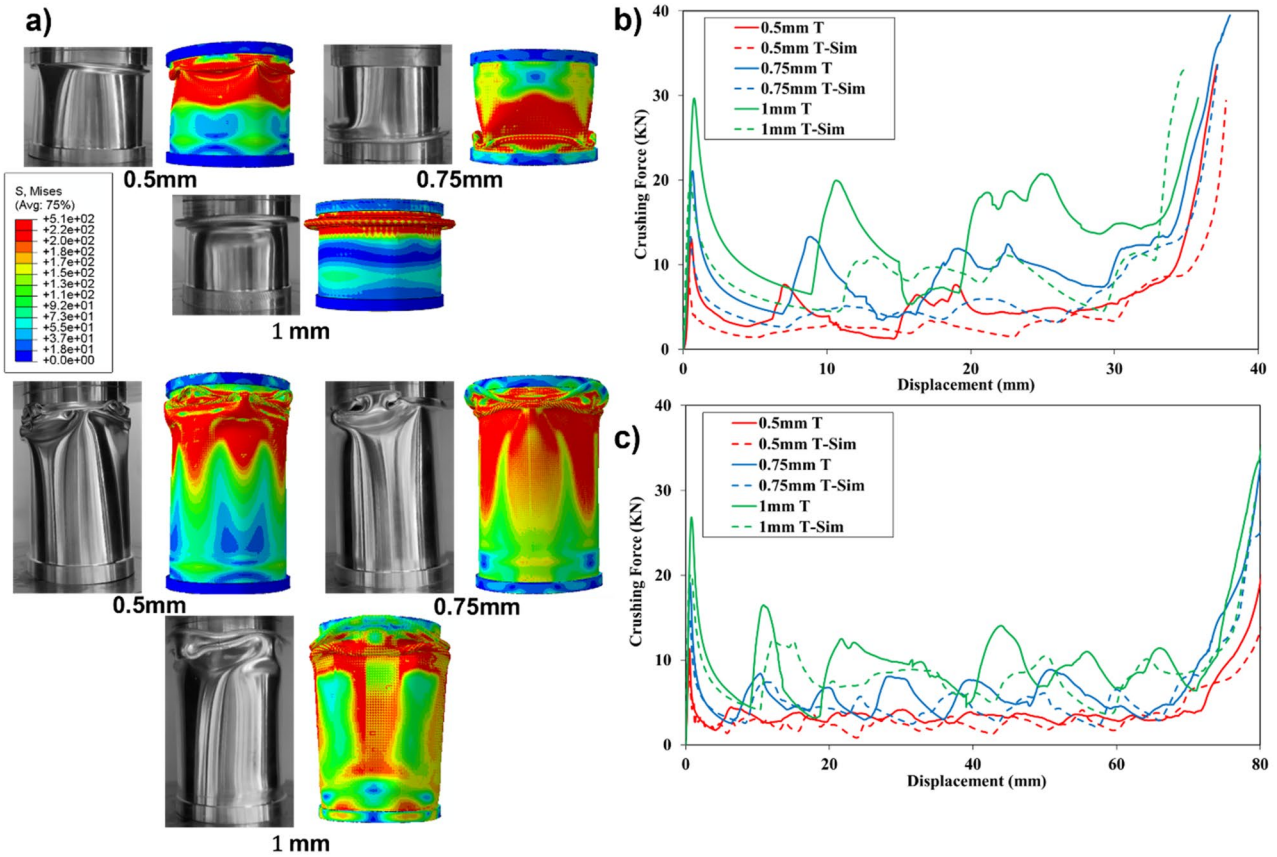

Fig. 4 Experimental vs computational model deformation behavior at 30% strain level showing von Mises stress contours in MPa for **a** short and long empty Al tubes and force–displacement curves for **b** short and **c** long tubes with different thicknesses. The dashed lines represent FEA results

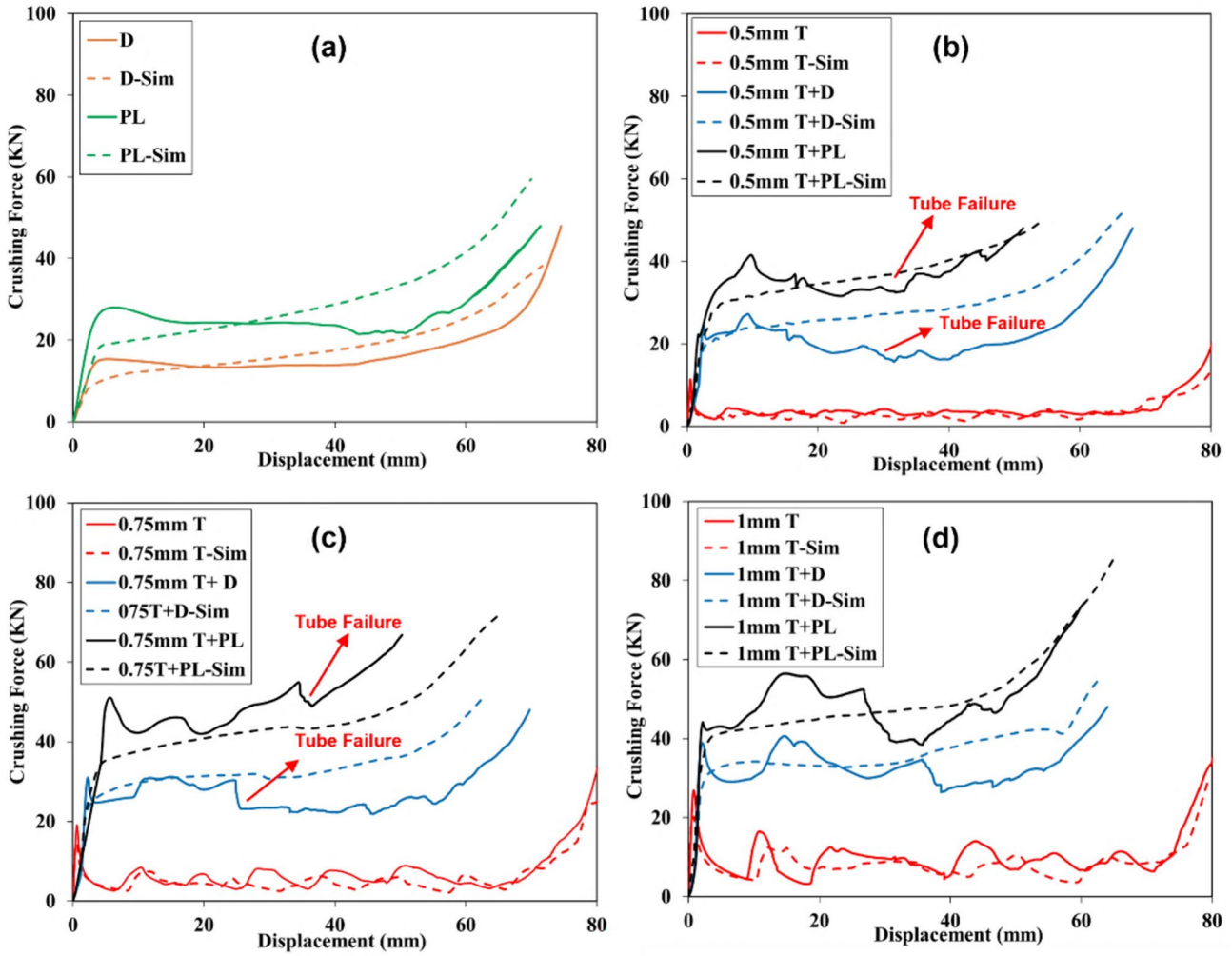

Fig. 5 Force–displacement curves for long samples: **a** core lattices; **b** 0.5 mm tubes; **c** 0.75 mm tubes; **d** 1 mm tubes. The dashed lines represent computational results

similar trend as the experimentally obtained ones. Stiffness, densification displacement, in addition to the plateau crushing force were well captured by the elasto-plastic material model for core structures and tubes (empty or filled). Since the inner lattice structure in the simulation was homogenized, the deformation mechanism differs from the experimentally obtained samples, which are shown by the perfectly plastic plateau in the simulation curves, as opposed to the fluctuating plateau in the experimental curves, which represents the deformation behavior of the inner core lattice.

It can be noted from the force–displacement curves that the addition of the inner core highly increased the forces developed in the structure, preventing the initial dip in the empty tubes' curves. Furthermore, the SC-FCC-BCC plate-lattice had higher stiffness and was able to sustain higher loads as compared to diamond. Generally, diamond TPMS structures have superior plateau and yield stresses as compared to individual plate-lattices [49]. In the current study, the plate-lattice had a higher design relative density ($\rho_R = 50\%$) as opposed to diamond lattice ($\rho_R = 40\%$), thus, can sustain higher loads. For all long samples, the addition of the core structure to the tube results in the reduction in the stiffness, which can be indicated by the slope in the elastic region. The value of the stiffness is an average of the empty tube and reference core structure. Interestingly, the addition of the lattice structures has a negligible effect on the stiffness for short samples. In particular, the slope of the force–displacement curve (i.e., stiffness) was identical for all three structures at any tube thickness. Tubes with low thickness were noted to fail at early loading stages. The failure displacement values of these tubes, extracted from crushing videos, is denoted in the plots.

To fully visualize the behavior of the hybrid structures and the interaction effect, the deformation mechanism of the long and short samples with different tube thicknesses

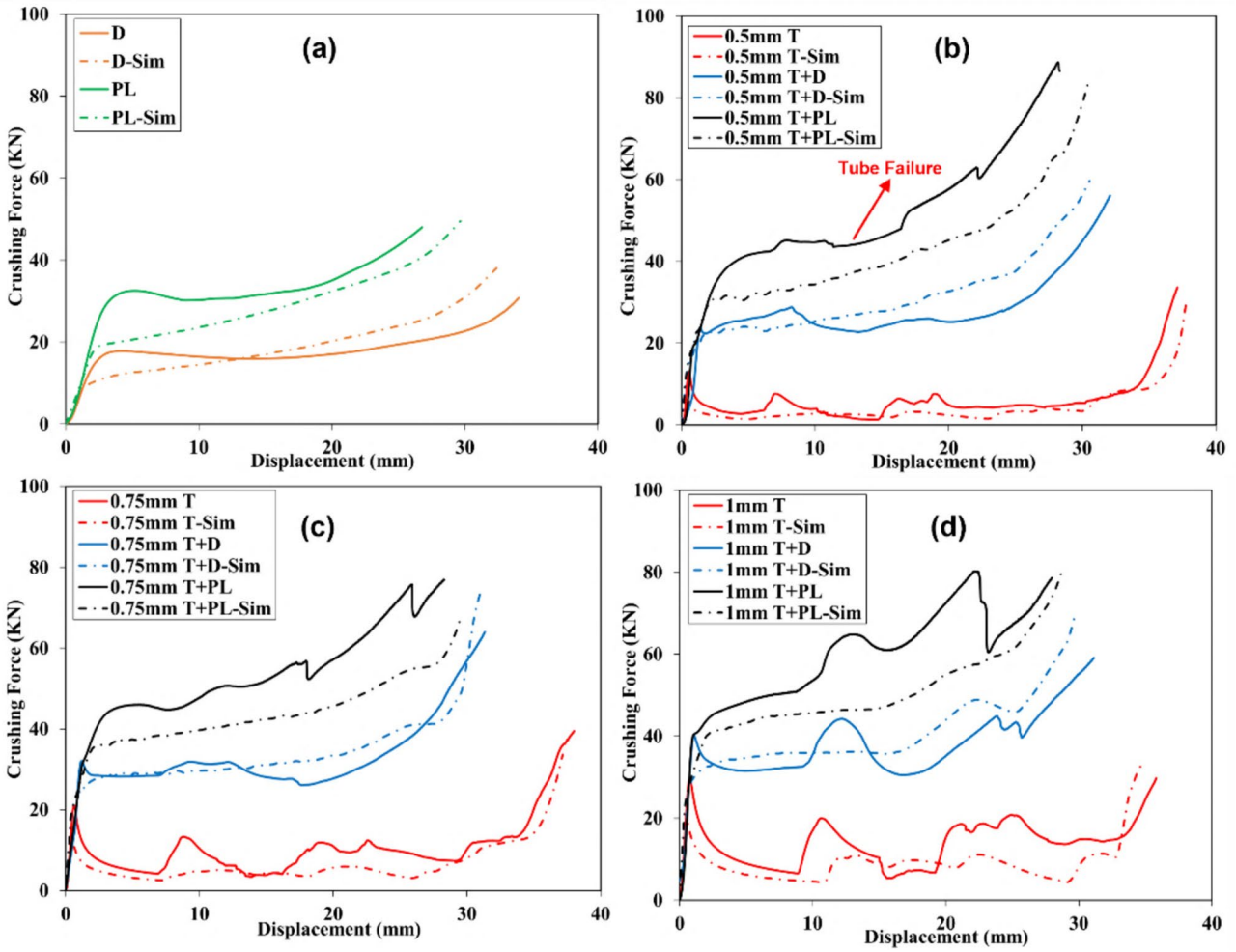

Fig. 6 Force–displacement curves for short samples: **a** core lattices; **b** 0.5 mm tubes; **c** 0.75 mm tubes; **d** 1 mm tubes. The dashed lines represent computational results

at 45% strain (45 mm and 22.5 mm displacement) are illustrated in Figs. 7 and 8, respectively.

As in the figures, the deformation mechanism for diamond and plate-lattice core structures had distinct deformation behavior for long and short samples. In particular, diamond cylindrical lattice develops shear bands in the diagonal direction in a 45° plane for both long and short samples, up to 20 mm displacement for long and 10 mm for short samples, while the constituting plates of the plate-lattice tend to bend towards the loading direction. Furthermore, for both diamond and plate-lattice cylinders, buckling due to the localization of the stress in the middle was observed. This buckling resulted in the early failure of the thin tubes when the core lattices were added ($t_T = 0.5$ and 0.75 mm), which was not detected as thicker tubes were utilized ($t_T = 1$ mm). For the short samples, on the other hand, buckling of the as-fabricated core structures was less noticeable, which was attributed to the ratio of L/D being minimized. As a result, failure of the samples at initial loading was only reported for structure with the diamond core at $t_T = 0.5$ and 0.75 mm tubes. The deformation mechanism of the thicker tubes that did not experience early failure appears to be different for long and short samples. At $t_T = 0.75$ and 1 mm, short tubes filled with plate-lattice and diamond lattice tended to form rings around the inner core. The formation of these rings is indicated in the force–displacement curves of Fig. 6c and d by two dips at the early loading stage (10–20 mm). The deformation behavior of the short hybrid structures was more stable than that of the long samples, which was highly reflected in the force–displacement curves. Particularly, the plateau stress was higher for short samples in most cases of the various design combinations.

3.1.2.2 Mechanical properties of the hybrid structures In this sub-section, the effects of tube thickness and height, in addition to the core lattice type on the mechanical properties extracted from the force–displacement response were discussed. One can convert the experimentally obtained force–displacement

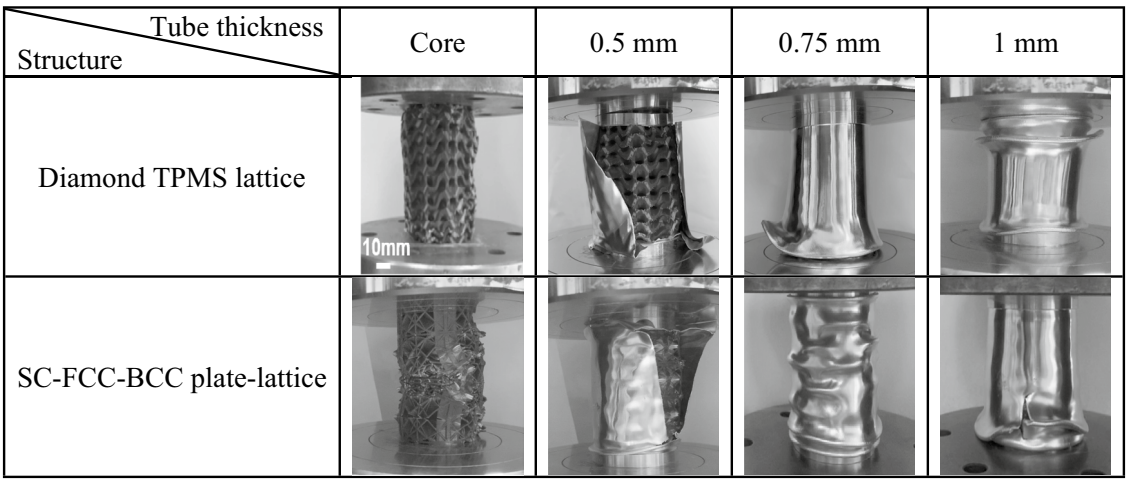

Fig. 7 Deformation mechanism of the long reference cores and hybrid structures with different thicknesses at 45 mm displacement (45% strain level)

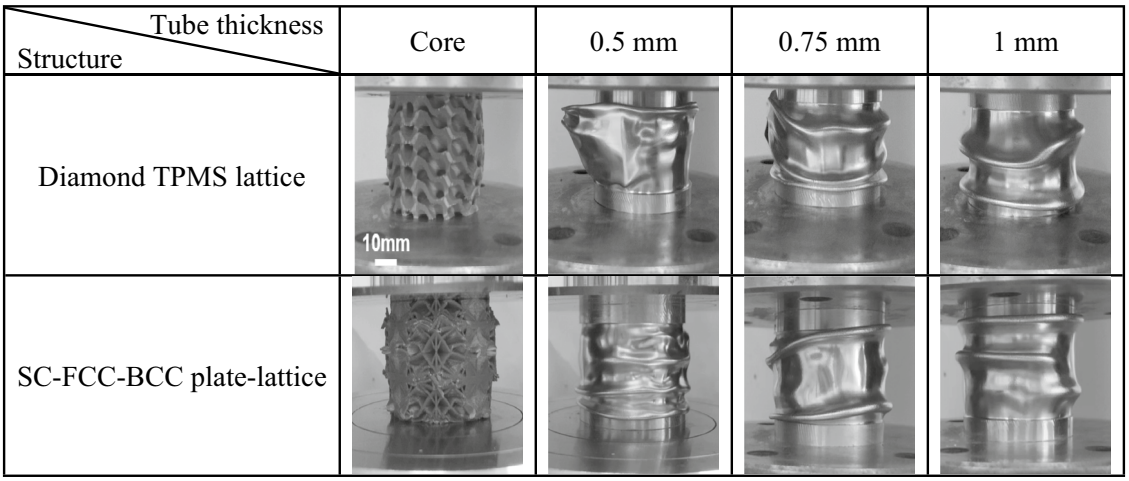

Fig. 8 Deformation mechanism of the short reference cores and hybrid structures with different thicknesses at 22.5 mm displacement (45% strain level)

diagrams into stress–strain responses by dividing the force by the cross-sectional area and displacement by the tube's length. Thus, the properties chosen to compare the mechanical properties were plateau stress, toughness, and SEA. The plateau stress was calculated as the average stress between the range 20% and 40% strain levels. While toughness was calculated as the area under the stress–strain curve up to the strain level representing the onset of densification. The densification strain determined varied from 60 to 75% strain level, depending on the sample. The specific toughness and SEA were calculated as follows:

$$\text{toughness} = \frac{\int_0^{\varepsilon_d} \sigma(\varepsilon)\mathrm{d}x}{m_m}, \tag{2}$$

$$\text{SEA} = \frac{\int_0^{\delta_d} F(x)\mathrm{d}x}{m_m}, \tag{3}$$

where ε_d and δ_d represent densification strain and displacement, respectively; F is the compressive force, and m_m is the measured mass of the sample.

The plateau stress values of the long and short samples, extracted from the curves, are provided in the bar charts of Fig. 9. The effect of tube thickness variation on the plateau stress was quite comparable for both short and long samples. The value of plateau stress increased with increase in tube thickness. This behavior was expected since thicker tube thickness allows the structure to sustain more load, and thus increases the plateau stress.

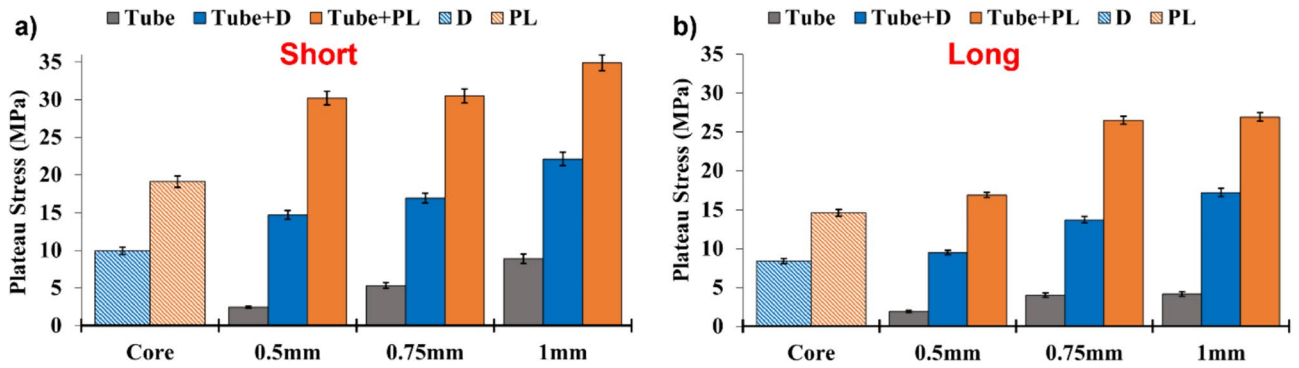

Fig. 9 Experimental plateau stress chart with error bars for **a** short and **b** long tubes

Variations in plateau stress were more substantial when tube height was varied, as opposed to tube thickness. Comparing long and short samples, plateau stress increased up to 70% for short samples than the long tubes. This huge variation can be directly correlated to the deformation mechanism of the structure, since the failure of the tube was less probable as tube height was reduced (Figs. 7 and 8). In a related study, Novak et al. [45] tested in situ and ex situ diamond TPMS-filled stainless steel squared tubes under axial loading. Contrary to our findings, the authors noted that plateau stress increased with tube height. The differences in their results were attributed to the variation in the deformation behavior between the current circular and their squared tubes, in addition to the difference in interactions between stainless steel-stainless steel material and ABS-aluminum material. The interaction effect between the two materials is illustrated in the toughness bar charts of Fig. 10.

The dashed red lines in the figure represent the sum of the toughness of the two structures (tube and core) calculated individually for different tube thicknesses. Having higher values of toughness above these lines for any structure shows the advantage of adding the core lattices to the tubes. For both short and long samples, the addition of the core lattice increased the toughness compared to empty tubes, but the interaction effect differs from one structure to another. In particular, hybrid structures with thin tubes ($t_T = 0.5$ mm) resulted in negligible interaction effect between the core and tube, and thus, a lower or equivalent value of toughness compared to the summed values was obtained. When larger thickness was utilized, the interaction effect was more noticeable, and higher ability to absorb the mechanical energy was achieved. This was likely to occur, since lower tube thicknesses typically result in early failure of the tube (Figs. 7 and 8). Interestingly, the diamond lattice-filled tubes demonstrated considerable toughness for 1 mm tubes, yet in the case of the 0.5 mm and 0.75 mm short tubes, the toughness did not reach the levels indicated by the red dashed line, contrary to the performance of the plate-lattice samples. This disparity is related to the failure of the diamond TPMS tube at an earlier loading stage as compared to the plate-lattice at equivalent tube thicknesses (Fig. 8). The variation arises from the intrinsic discrepancies in the architectural designs of the two lattice types. Although the diamond TPMS typically shows effectiveness in energy absorption, it

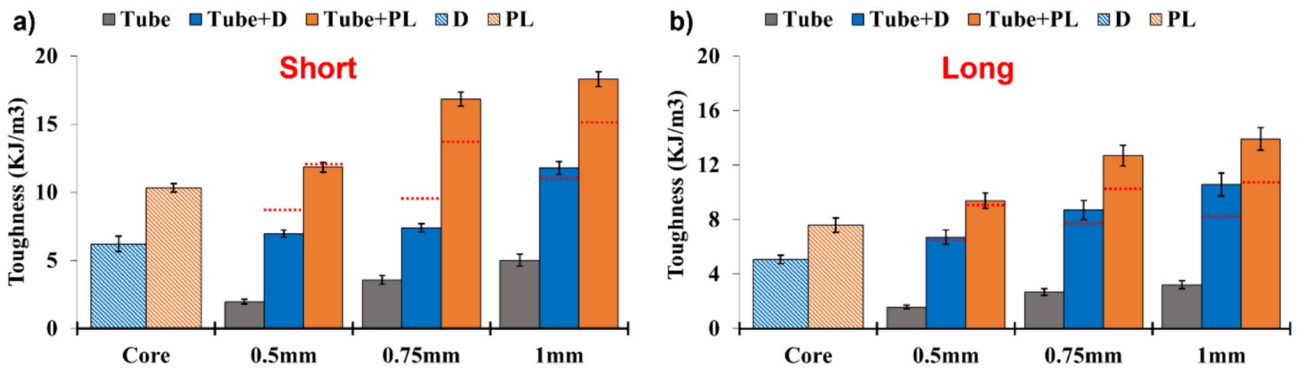

Fig. 10 Experimental specific toughness chart with error bars for **a** short and **b** long samples. The dashed red lines represent individual toughness summation of the two structures

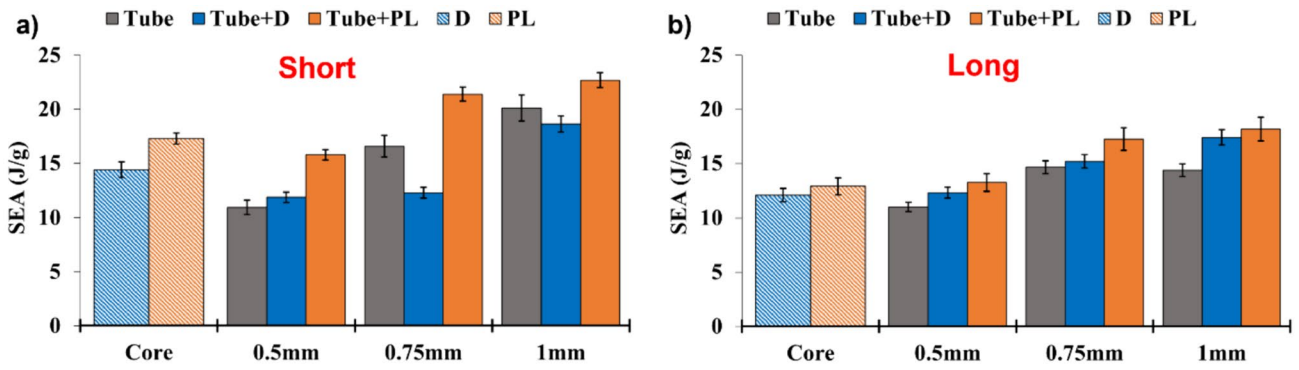

Fig. 11 Experimental specific energy absorption (SEA) charts with error bars for **a** short and **b** long samples

lacks the even stress distribution seen in the SC-FCC-BCC plate-lattice, leading to more noticeable buckling that compromises the tube's structural integrity at lower thicknesses. Broadly speaking, the toughness of the short samples was much higher than the long ones, which was due to the ability of the structures to sustain higher plateau stresses (Fig. 9). Additionally, the SEA charts for short and long samples are presented in Fig. 11a and b, respectively.

For both short and long samples, the SEA was higher for the plate-lattice hybrid structures at any tube thickness considered, compared to diamond structures, which indicates a more reliable ability of the plate-lattice than diamond to sustain load and absorb mechanical energy. In general, short samples had greater values of SEA than long samples, which is related to the lower buckling of the inner tubes and the more stable deformation mechanism for the 50 mm long tubes as compared to 100 mm. The maximum SEA obtained for diamond short hybrid structures was 18.6 J/g at 1 mm tube thickness, while the plate-lattice reached a maximum of 22.7 J/g at the same thickness. The relative increase in SEA was maximum for diamond long samples with $t_T = 1$ mm tube, showing an increase of 21%. While for the plate-lattice, the increase in SEA against the empty reference tubes was maximum for short samples with up to 44%. These variations were directly related to the interaction effects between the inner core and the tube, noted in the deformation mechanism of Figs. 7 and 8, with tubes undergoing formation of circular rings.

4 Conclusions

In this paper, the mechanical behavior of diamond TPMS and SC-FCC-BCC plate-lattice ex situ filled aluminum tubes was investigated experimentally and compared with finite element analyses. Besides filled tubes, the constituent structures were also tested (i.e., empty tubes and as-fabricated core lattices). The structures were analyzed at different combinations of tube lengths ($h_T = 50$, 100 mm) and thicknesses ($t_T = 0.5$, 0.75, 1 mm), based on a factorial design. The design of the hybrid structure played a critical role in determining the deformation behavior. Additionally, the mechanical behavior of both long and short empty tubes, as predicted by the computational model using the homogenization technique, closely aligned with experimental results, and was achieved at a lower computational cost. Experimental results revealed that diamond cylindrical lattices develop diagonal shear bands at the early loading stages, while the constituting plates of the plate-lattice tend to bend towards the loading direction. Both structures suffered from stress localization initiated at the center of the samples, which resulted in different degrees of buckling. For all considered structures, short samples showed higher capabilities to absorb energy as compared to long samples, due to their lower degree of buckling. Those capabilities were reflected in the plateau stress and toughness curves. The force–displacement curves demonstrated an interaction effect between the cores and tubes, influenced by the lattice design and tube thickness. This effect was a result of the variations in the deformation mechanism, which subsequently varied the energy absorption of the structures. From an energy absorption point of view, the optimal hybrid structure design with maximum SEA was found to be at 1 mm short tube samples for both SC-FCC-BCC plate-lattice (22.7 J/g) and diamond TPMS (18.6 J/g), suggesting the potential of their utilization in impact resistance applications.

Acknowledgements This publication is based upon work supported by the Khalifa University (KU) under Award No. RCII-2019-003.

Data availability The data will be available upon request.

Declarations

Conflict of interest The authors have no financial or proprietary interests in any material discussed in this article.

References

1. Meshreki M, Kövecses J, Attia H, Tounsi N (2008) Dynamics modeling and analysis of thin-walled aerospace structures for fixture design in multiaxis milling. J Manuf Sci Eng 130:0310111–03101112. https://doi.org/10.1115/1.2927444
2. Demirci E, Yildiz AR (2018) An experimental and numerical investigation of the effects of geometry and spot welds on the crashworthiness of vehicle thin-walled structures. Mater Test 60:553–561. https://doi.org/10.3139/120.111187
3. Alavi Nia A, Parsapour M (2013) An investigation on the energy absorption characteristics of multi-cell square tubes. Thin-Walled Struct 68:26–34. https://doi.org/10.1016/j.tws.2013.01.010
4. Lv J, Bai Z, Du X et al (2022) Crashworthiness design of 3D lattice-structure filled thin-walled tubes based on data mining. Int J Crashworthiness. https://doi.org/10.1080/13588265.2022.2101306
5. Alghamdi AAA (2001) Collapsible impact energy absorbers: an overview. Thin-Walled Struct 39:189–213. https://doi.org/10.1016/S0263-8231(00)00048-3
6. Wu J, Zhang Y, Zhang F et al (2021) A bionic tree-liked fractal structure as energy absorber under axial loading. Eng Struct 245:1129414. https://doi.org/10.1016/j.engstruct.2021.112914
7. Olabi AG, Morris E, Hashmi MSJ (2007) Metallic tube type energy absorbers: a synopsis. Thin-Walled Struct 45:706–726. https://doi.org/10.1016/j.tws.2007.05.003
8. Zarei HR, Kröger M (2008) Optimization of the foam-filled aluminum tubes for crush box application. Thin-Walled Struct 46:214–221. https://doi.org/10.1016/j.tws.2007.07.016
9. Liang H, Zhao Y, Chen S et al (2023) Review of Crashworthiness studies on cellular structures. Automot Innov 6:379–403. https://doi.org/10.1007/s42154-023-00237-0
10. Shinde RB, Mali KD (2018) An overview on impact behaviour and energy absorption of collapsible metallic and non-metallic energy absorbers used in automotive applications. IOP Conf Ser Mater Sci Eng 346:41. https://doi.org/10.1088/1757-899X/346/1/012054
11. Chahardoli S, Akhavan Attar A, Ghorbanhosseini S, Hossaeini Marashi SM (2021) Investigation of the bending and crushing for the light-weight structures used in vehicle's radiator. Mech Based Des Struct Mach 2021:1–17. https://doi.org/10.1080/15397734.2021.1967165
12. Santhosh-Kumar V, Manikandaraja G (2016) Numerical study on energy absorbing characteristics of thin-walled tube under axial and oblique impact. Alexandr Eng J. https://doi.org/10.1016/j.aej.2015.12.008
13. Ataollahi S (2023) A review on additive manufacturing of lattice structures in tissue engineering. Bioprinting 35:e00304. https://doi.org/10.1016/j.bprint.2023.e00304
14. Park JW, Park H, Kim JH et al (2022) (2022) Fabrication of a lattice structure with periodic open pores through three-dimensional printing for bone ingrowth. Sci Rep 121(12):1–8. https://doi.org/10.1038/s41598-022-22292-z
15. Babbage JM, Mallick PK (2005) Static axial crush performance of unfilled and foam-filled aluminum-composite hybrid tubes. Compos Struct 70:177–184. https://doi.org/10.1016/j.compstruct.2004.08.021
16. Sun G, Wang Z, Yu H et al (2019) Experimental and numerical investigation into the crashworthiness of metal-foam-composite hybrid structures. Compos Struct 209:535–547. https://doi.org/10.1016/j.compstruct.2018.10.051
17. Abada M, Ibrahim A (2020) Hybrid multi-cell thin-walled tubes for energy absorption applications: blast shielding and crashworthiness. Compos Part B Eng 183:107720. https://doi.org/10.1016/j.compositesb.2019.107720
18. Reuter C, Tröster T (2017) Crashworthiness and numerical simulation of hybrid aluminium-CFRP tubes under axial impact. Thin-Walled Struct 117:1–9. https://doi.org/10.1016/j.tws.2017.03.034
19. Luo C, Han CZ, Zhang XY et al (2021) Design, manufacturing and applications of auxetic tubular structures: a review. Thin-Walled Struct 163:107682. https://doi.org/10.1016/j.tws.2021.107682
20. Guillow SR, Lu G, Grzebieta RH (2001) Quasi-static axial compression of thin-walled circular aluminium tubes. Int J Mech Sci 43:2103–2123. https://doi.org/10.1016/S0020-7403(01)00031-5
21. Fu X, Zhang X, Huang Z (2021) Axial crushing of Nylon and Al/Nylon hybrid tubes by FDM 3D printing. Compos Struct 256:113055. https://doi.org/10.1016/j.compstruct.2020.113055
22. Sun G, Chen D, Zhu G, Li Q (2022) Lightweight hybrid materials and structures for energy absorption: a state-of-the-art review and outlook. Thin-Walled Struct 172:108760. https://doi.org/10.1016/j.tws.2021.108760
23. Zhang Y, Sun G, Li G et al (2012) Optimization of foam-filled bitubal structures for crashworthiness criteria. Mater Des 38:99–109. https://doi.org/10.1016/j.matdes.2012.01.028
24. Hanssen AG, Langseth M, Hopperstad OS (2000) Static and dynamic crushing of square aluminum extrusions with aluminum foam filler. Int J Impact Eng 24:347–383. https://doi.org/10.1016/S0734-743X(99)00169-4
25. Li Z, Lu F (2015) Bending resistance and energy-absorbing effectiveness of empty and foam-filled thin-walled tubes. J Reinf Plast Compos 34:761–768. https://doi.org/10.1177/0731684415580329
26. Berger JB, Wadley HNG, McMeeking RM (2017) Mechanical metamaterials at the theoretical limit of isotropic elastic stiffness. Nature 543:533–537. https://doi.org/10.1038/nature21075
27. Kladovasilakis N, Tsongas K, Tzetzis D (2021) Mechanical and fea-assisted characterization of fused filament fabricated triply periodic minimal surface structures. J Compos Sci 5:58. https://doi.org/10.3390/jcs5020058
28. Almesmari A, Sheikh-Ahmad J, Jarrar F, Bojanampati S (2023) Optimizing the specific mechanical properties of lattice structures fabricated by material extrusion additive manufacturing. J Mater Res Technol 22:1821–1838. https://doi.org/10.1016/j.jmrt.2022.12.024
29. Al-Ketan O, Soliman A, AlQubaisi AM, Abu Al-Rub RK (2018) Nature-inspired lightweight cellular co-continuous composites with architected periodic gyroidal structures. Adv Eng Mater 20:1700549. https://doi.org/10.1002/adem.201700549
30. Liu Y (2021) Mechanical properties of a new type of plate–lattice structures. Int J Mech Sci 192:106141. https://doi.org/10.1016/j.ijmecsci.2020.106141
31. Tabacu S, Ducu C (2018) Experimental testing and numerical analysis of FDM multi-cell inserts and hybrid structures. Thin-Walled Struct 129:197–212. https://doi.org/10.1016/j.tws.2018.04.009
32. Alagha AN, Hussain S, Zaki W (2021) Additive manufacturing of shape memory alloys: A review with emphasis on powder bed systems. Mater Des 204:109654. https://doi.org/10.1016/j.matdes.2021.109654
33. Liu Q, Mo Z, Wu Y et al (2016) Crush response of CFRP square tube filled with aluminum honeycomb. Compos Part B Eng 98:406–414. https://doi.org/10.1016/j.compositesb.2016.05.048
34. Simpson J, Kazancı Z (2020) Crushing investigation of crash boxes filled with honeycomb and re-entrant (auxetic) lattices. Thin-Walled Struct 150:106673. https://doi.org/10.1016/j.tws.2020.106676
35. Hussein RD, Ruan D, Lu G et al (2017) Crushing response of square aluminium tubes filled with polyurethane foam and aluminium honeycomb. Thin-Walled Struct 110:140–154. https://doi.org/10.1016/j.tws.2016.10.023

36. Surace R, De Filippis LAC, Ludovico AD, Boghetich G (2010) Application of Taguchi method for the multi-objective optimization of aluminium foam manufacturing parameters. Int J Mater Form 3:1–5. https://doi.org/10.1007/s12289-009-0409-9
37. Liu Z, Liu P, Huang W et al (2020) Mechanical and failure behaviors of lattice-plate hybrid structures. MRS Commun 10:42–54. https://doi.org/10.1557/mrc.2019.153
38. Cetin E, Baykasoğlu C (2019) Energy absorption of thin-walled tubes enhanced by lattice structures. Int J Mech Sci 157–158:471–484. https://doi.org/10.1016/j.ijmecsci.2019.04.049
39. Cetin E, Baykasoğlu C (2020) Crashworthiness of graded lattice structure filled thin-walled tubes under multiple impact loadings. Thin-Walled Struct 154:10684. https://doi.org/10.1016/j.tws.2020.106849
40. Baykasoğlu A, Baykasoğlu C, Cetin E (2020) Multi-objective crashworthiness optimization of lattice structure filled thin-walled tubes. Thin-Walled Struct 149:412. https://doi.org/10.1016/j.tws.2020.106630
41. Liu H, Chng ZXC, Wang G, Ng BF (2021) Crashworthiness improvements of multi-cell thin-walled tubes through lattice structure enhancements. Int J Mech Sci 210:896. https://doi.org/10.1016/j.ijmecsci.2021.106731
42. Al-Ketan O, Abu Al-Rub RK, Rowshan R (2018) The effect of architecture on the mechanical properties of cellular structures based on the IWP minimal surface. J Mater Res 33:343–359. https://doi.org/10.1557/jmr.2018.1
43. Al-Ketan O, Rowshan R, Abu Al-Rub RK (2018) Topology-mechanical property relationship of 3D printed strut, skeletal, and sheet based periodic metallic cellular materials. Addit Manuf 19:167–183. https://doi.org/10.1016/J.ADDMA.2017.12.006
44. Xue R, Cui X, Zhang P et al (2020) Mechanical design and energy absorption performances of novel dual scale hybrid plate-lattice mechanical metamaterials. Extrem Mech Lett 40:100918. https://doi.org/10.1016/j.eml.2020.100918
45. Novak N, Kytyr D, Rada V et al (2022) Compression behaviour of TPMS-filled stainless steel tubes. Mater Sci Eng A 852:143680. https://doi.org/10.1016/j.msea.2022.143680
46. Novak N, Al-Ketan O, Krstulović-Opara L et al (2022) Bending behavior of triply periodic minimal surface foam-filled tubes. Mech Adv Mater Struct 2022:1–14. https://doi.org/10.1080/15376494.2022.2068207
47. Yin H, Guo D, Wen G, Wu Z (2022) On bending crashworthiness of smooth-shell lattice-filled structures. Thin-Walled Struct 171:145. https://doi.org/10.1016/j.tws.2021.108800
48. Alagha AN, Nguyen V, Zaki W (2022) Effective phase transformation behavior of NiTi triply periodic minimal surface architectures. J Intell Mater Syst Struct 34:672–695. https://doi.org/10.1177/1045389X221115704
49. Almesmari A, Alagha AN, Naji MM et al (2023) Recent advancements in design optimization of lattice-structured materials. Adv Eng Mater 25:2201780. https://doi.org/10.1002/ADEM.202201780
50. Al-Ketan O, Abu Al-Rub RK (2021) MSLattice: a free software for generating uniform and graded lattices based on triply periodic minimal surfaces. Mater Des Process Commun 3:e205. https://doi.org/10.1002/mdp2.205
51. Alagha AN, Almesmari A, Sheikh-Ahmed J et al (2024) On the mechanical behavior and energy absorption of TPMS and plate-lattices. J Eng Mech 13:3882
52. Gordeev EG, Galushko AS, Ananikov VP (2018) Improvement of quality of 3D printed objects by elimination of microscopic structural defects in fused deposition modeling. PLoS ONE 13:e0198370. https://doi.org/10.1371/journal.pone.0198370
53. Li QM, Magkiriadis I, Harrigan JJ (2006) Compressive strain at the onset of densification of cellular solids. J Cell Plast 42:371–392. https://doi.org/10.1177/0021955X06063519
54. Lee DW, Khan KA, Abu Al-Rub RK (2017) Stiffness and yield strength of architectured foams based on the Schwarz Primitive triply periodic minimal surface. Int J Plast 95:1–20. https://doi.org/10.1016/j.ijplas.2017.03.005
55. Andrews KRF, England GL, Ghani E (1983) Classification of the axial collapse of cylindrical tubes under quasi-static loading. Int J Mech Sci 25:687–696. https://doi.org/10.1016/0020-7403(83)90076-0